An integrin-targeting AAV developed using a novel computational rational design methodology presents improved targeting of the skeletal muscle and reduced liver tropism

Ai Vu Hong (avuhong@genethon.fr)
Genethon https://orcid.org/0000-0002-0872-4295
Laurence Suel
Genethon
Jérôme Poupiot
Genethon
Isabelle Richard
Genethon

Article

Keywords:

Posted Date: October 27th, 2023

DOI: https://doi.org/10.21203/rs.3.rs-3466229/v1

Additional Declarations: Yes there is potential Competing Interest. A.H.V. and I.R. are inventors on PCT application EP2023/065499 for the integration of RGDLxxL/I motif in AAV capsid for enhanced muscle transduction efficiency. I.R. is a part-time employee of Atamyo Therapeutics. The other authors declare no competing interests.

Abstract

Current adeno-associated virus (AAV) gene therapy using nature-derived AAVs is limited by non-optimal tissue targeting. In the treatment of muscular diseases (MD), high doses are therefore often required, but can lead to severe adverse effects. To lower treatment doses, we rationally designed an AAV that specifically targets skeletal muscle. We employed a novel computational design that integrated binding motifs of integrin alpha V beta 6 (αVβ6) into a liver-detargeting AAV capsid backbone to target the human αVβ6 complex – a selected AAV receptor for skeletal muscle. After sampling the low-energy capsid mutants, all *in silico* designed AAVs showed higher productivity compared to their parent. We confirmed *in vitro* that the enhanced transduction is due to the binding to the αVβ6 complex. Thanks to inclusion of αVβ6-binding motifs, the designed AAVs exhibited enhanced transduction efficacy in human differentiated myotubes as well as in murine skeletal muscles *in vivo*. One notable variant, LICA1, showed similar muscle transduction to other published myotropic AAVs, while being significantly more strongly liver-detargeted. We further examined the efficacy of LICA1, in comparison to AAV9, in delivering therapeutic transgenes in two mouse MD models at a low dose of 5E12 vg/kg. At this dose, AAV9 was suboptimal, while LICA1 transduced effectively and significantly better than AAV9 in all tested muscles. Consequently, LICA1 corrected the myopathology, restored global transcriptomic dysregulation, and improved muscle functionality. These results underline the potential of our design method for AAV engineering and demonstrate the relevance of the novel AAV variant for gene therapy treatment of MD.

One Sentence Summary

We developed a novel computationally AAV design method resulting in a new myotropic AAV, which allows low-dose AAV treatment for muscular dystrophies.

INTRODUCTION

Over 50 years since their discovery, adeno-associated viruses (AAVs) have shown great promise as an effective viral vector for gene delivery and gene therapy, leading to recent approval of therapeutic products [1, 2]. Due to unmet medical needs and natural AAV tropism, many AAV-based gene therapies focus on treating muscle diseases (MD) [3]. Systemic treatment in such diseases aims to primarily target skeletal muscle, which accounts for more than 40% of body mass, and therefore often requires very high doses (≥1E14 vg/kg) to achieve meaningful therapeutic efficacy [3-6]. In addition, most recombinant AAVs built on natural-occurring variants lack specificity and often accumulate in the liver, with the concomitant risk of hepatotoxicity [7]. Other key challenges of rAAV use persist, including manufacturing, immunological barriers, and associated toxicity [1, 2, 8, 9].

AAV is a small non-pathogenic single-stranded DNA parvovirus. Multiple open reading frames (ORFs) were identified in its genome, including *Rep*, *Cap*, *AAP* and *MAAP* [1, 10]. The single *Cap* ORF expresses three capsid proteins - virion protein 1 (VP1), VP2 and VP3, which assemble into an icosahedral 60-mer capsid. Structurally, the VP3 monomer core contains a highly conserved eight-stranded β-barrel motif [11].

Inserted between the β-strands, nine surface-exposed variable regions (VR1-9) result in local topological differences between serotypes and dictate virus-host interaction. Consequently, genetically modifying VRs can drastically change the AAV, transduction, antigenic profile, and fitness [10, 12, 13]. VR4 and VR8, that cluster together spatially, forming the most prominent protrusion at the 3-fold axis, have been widely subjected to modifications, notably by inserting short peptides into the loop apices [14]. This resulted in some highly efficient capsid variants for transducing a variety of cell types and tissues [1, 12]. Among these, remarkably, AAVMYOs [15, 16] and MYOAAVs [17] transduce skeletal muscles, deliver therapeutic transgenes efficiently, and were shown to correct dystrophic phenotypes in MD mouse models at relatively low doses (2E12 – 1E13 vg/kg).

Importantly, the myotropic AAVs [15-17] identified by muscle-directed high-throughput screening (HTS) were shown to share an Arg-Gly-Asp (RGD) motif, presumably targeting the integrin complex [17-20]. Integrins are a group of heterodimeric proteins composed of an α- and a β subunit that serve various cellular functions, including cell adhesion, cell migration, and cell signaling [21]. As adhesion molecules, integrins also mediate cell-pathogen interactions, and are therefore exploited by many viruses, including natural AAV, to infect cells [22-24]. Indeed, many of these viruses use an RGD motif on their viral envelope glycoproteins or capsids for cell attachment, endocytosis, entry, and endosomal escape [18, 22, 25]. The discovery that RGD-dependent integrin-targeting AAV variants can acquire myotropism therefore represents a novel potential candidate approach for a rational design to target skeletal muscle.

This study introduces a novel computational method for a rational AAV design targeting skeletal muscle, which resulted in a novel myotropic vector for MD gene therapy. First, the human skeletal muscle-enriched integrin complex alpha V beta 6 (αVβ6) was selected as the target receptor. Inspired by one-sided protein design [26, 27], we computationally designed a previously developed liver-detargeting hybrid capsid between AAV9 and AAVrh74 (Cap9rh74) as an αVβ6 binder. The VR4 loop was completely modified, in which new sequences were iteratively selected to simultaneously optimize for free energy, while hosting αVβ6-binding RGDLXXL/I motifs. All designed AAVs were well-produced, at higher titers than their parent. The designed AAVs were confirmed to require αVβ6 binding for cellular transduction. The most promising variant, renamed LICA1, was selected for further analysis and showed superior transduction in human differentiated myotubes and strong myotropism in several mouse models. We evaluated this variant by delivering therapeutic transgenes in two MD mouse models at a very low dose of 5E12 vg/kg, in comparison to AAV9. In both cases, LICA1 presents higher efficacy than AAV9 in correcting dystrophic phenotypes, global transcriptomic changes and restoring muscle function, thanks to improved transduction and transgene expression in skeletal muscles. Collectively, the study provides a proof-of-concept for a new rational AAV design pipeline leveraging protein design tools, which resulted in a novel myotropic AAV with high potential for gene therapy for muscle diseases.

RESULTS

1. Selection of the cellular receptor for rational design

Several myotrophic AAVs have recently been developed, notably, the insertion into the AAV9 VR-VIII loop of P1 peptide (RGDLGLS) [15,16], and a series of RGD-containing sequences identified by directed evolution [17]. Importantly, these modified capsids shared a common RGD motif, which suggested their affinity to integrin (ITG), cell-surface heterocomplexes that interact with the extracellular matrix [28]. Using publicly available datasets, we aimed to select relevant integrin subunits for a subsequent rational AAV design targeting skeletal muscle.

Chemello and colleagues previously performed single-nucleus RNA sequencing, comparing gene expression of all cell types in the skeletal muscle of wild-type (WT) and Duchenne muscular dystrophy mouse models (D51) [29]. We extracted RNA levels of all integrin alpha and beta genes from these data (**Figure S1A**). Among all subunits, only the α- subunits *Itgav*, *Itga7* and the β-subunits *Itgb6*, *Itgb1*, and *Itgb5* show relatively high expression in the myogenic nuclei. Of interest is the fact that the expression level of *Itgb6* is highly enriched in myonuclei, and significantly upregulated in the dystrophic condition, whereas *Itgb1* and *Itgb5* expression are ubiquitous in all cell types, and significantly lower than the *Itgb6* level in all myonuclei. Among the two expressed α-subunits, only *Itgav* was known to associate with *Itgb6* to form αvβ6 heterocomplexes – a member of the RGD-binding integrin family [30]. Furthermore, bulk RNA sequencing data from multiple human tissues confirmed high expression of *Itgav* and *Itgb6* in skeletal muscle, and low expression of *Itgb6* in the liver and spleen, two preferred targets of natural AAV (**Figure S1B**, GTEx V8, dbGaP Accession phs000424.v8.p2). We therefore hypothesize that AAV transduction in skeletal muscle can be improved by rationally designing an AAV capsid that specifically binds to αvβ6.

2. Rational design of a hybrid capsid, Cap9rh74, with a high affinity to the αVβ6 complex

As we aim to specifically target the skeletal muscle, we selected a hybrid capsid that we previously developed and that has a liver-detargeting property as the parental capsid in our design (Patent Number: EP18305399.0). This hybrid capsid of AAV9 and AAV.rh74 (AAV9rh74) was constructed by replacing the AAV9 sequence of VR4 to VR8 with that of AAV-rh74. The hybrid capsid showed similar infectivity in skeletal and cardiac muscles but was strongly de-targeted from the liver. The latter property is of particular interest in skeletal muscle gene transfer since the majority of administrated viral vector will not accumulate in the liver, as is the case for natural AAVs [31,32].

After selection of the cellular receptor of interest and capsid backbone, AAV capsids were computationally engineered (**Fig. 1A**). First, the 3D structure of the parental capsid, of with structure was unknown, was modeled using AlphaFold2 [33,34]. The structural prediction of the Cap9rh74 aa 219–737 monomer performed using AlphaFold2 was at a high level of confidence, with predicted local distance difference test (lDDT-Cα), a per-residue measure of local confidence, of 97.04 and low predicted aligned error (PEA) of 4.32 (**Fig S1C-D**). This structure is thus suitable for the next steps in the design.

Second, we extracted the 3D structure or sequences of binding motifs of the human integrin complex from PDB. Importantly, αVβ6 was previously shown to bind with high affinity to the RGDLXXL/I motif found in the human TGF-β1 and TGF-β3 prodomains [35,36]. Binding peptides with eight amino acid

residues, aa214-221 in TGF-β1 (PDB: 5ffo) and aa240-247 in TGF-β3 (PDB: 4um9), were isolated from the corresponding crystal structures before grafting into the Cap9rh74 VR4 loop. Both motifs bind to αVβ6 dimer at a very similar position (**Fig S1E**).

Third, the defined binding motifs were then grafted into the VR4 loop (residues 453–459) of the capsid protein based on the RosettaRemodel protocol [37]. In the grafting-remodel process, many rounds of backbone optimization and sequence design iteratively search for low-energy sequence–structure pairs (**Fig. 1B**). The lowest-energy designs in grafting experiments of each TGF-β motif showed convergence in both structure and sequence (**Fig. 1C-D, S1F-G**). The new VR4 loops include the binding peptide and two flanking 2-amino acid linkers and retain the LXXL/I motif as an α-helix, which is important to bind in the β6 subunit's pocket [36].

Retrospective docking simulations of the two AAV_ITGs with the best scores, namely Cap9rh74_5ffo and Cap9rh74_4um9, on the αVβ6 complex showed highly similar binding positions of the new VR4 loop to its corresponding inserted motifs (**Fig. 1E-F**). This suggests that the new capsids can bind to αVβ6 thanks to VR4-included RGDLXXL/I motif. Sequences with the best scores, which reflect the thermodynamic stability of one static protein conformation [38], were subjected to experimental validation.

3. All designed AAV_ITGs showed higher productivity and enhanced cellular transduction via αVβ6 binding.

The two AAVs with the best design were then tested for productivity and the effectiveness of using αVβ6 as a cellular receptor. They were produced by tri-transfection with pITR-CMV-GFP-Luciferase as the expression cassette. Thanks to energy optimization, all the designed AAV-ITG variants significantly increase their titers compared to their parental hybrid capsid, to levels similar to those for AAV9 (**Fig. 2A, S2A**). In addition, all modified AAV-ITG variants retain proportions of VP1, VP2, VP3 capsid proteins with a similar ratio of AAV9 (**Fig. 2B**). This suggests that the designed sequences result in more stable AAV capsid complexes thanks to their estimated low energy structure, and therefore better production efficacy.

Next, we examined whether these AAV-ITGs can effectively use αVβ6 as a cellular receptor upon infection. First, a HEK293 cell line (293_αVβ6) constitutively overexpressing both integrin subunits, αV and β6, was created using the PiggyBac system (**Fig S2B-C**). The designed AAVs were then tested for their infectivity in this cell line. As expected, infection of AAV_ITGs in 293_αVβ6 cells, as defined by vector copy numbers (VCN), was higher than for AAV9 and AAV9rh74 (**Fig. 2C**). Both AAV_ITGs dramatically improved the luciferase activity ($FC_{9rh74\_4um9/AAV9}$=60.50, $FC_{9rh74\_5ffo/AAV9}$=25.99, $FC_{9rh74\_4um9/9rh74}$=63.99, and $FC_{9rh74\_4um9/9rh74}$=27.49, **Fig. 2D**). To investigate how specific AAV_ITGs used αVβ6 as a cellular receptor, we tested their infectivity under binding competition conditions. The number of AAV_ITG viral vectors entering the cells was significantly reduced when blocked by the recombinant protein αVβ6 before viral infection, but no change occurred with AAV9 or AAV9rh74 (**Fig. 2E**). This result suggests that efficient transduction of AAV_ITGs requires specific binding to a αVβ6 complex.

During myogenesis, αVβ6 is only expressed in late differentiation, but not in the myoblast stage (**Fig S1A, S2D**). We therefore hypothesized an enhanced transduction of AAV_ITGs in differentiated myotubes, but not myoblasts. We infected both human myoblasts and myotubes with AAV_ITGs. Low levels of luciferase activity were observed in all AAVs tested in human myoblasts (**Fig. 2G,I**). On the other hand, in human differentiated myotubes (hMT), VCN and luciferase activities in both AAV9rh74_4um9 and _5ff0 were significantly higher than for AAV9 or AAV9rh74 (**Fig. 2F,H,K**). In particular, variant AAV9rh74_4um9 showed a 16.56 ($p < 0.0001$) and 25.02-fold ($p < 0.0001$) improvement in luciferase activity compared to AAV9 and AAV9rh74, respectively, which is in agreement with its superior transduction efficiency and transgene expression seen in 293_αVβ6 cells.

In summary, the two designed AAV_ITGs were both well-produced and function via αVβ6-specific binding, thus enhancing their transduction efficiency in 293_αVβ6 and human differentiated myotubes.

4. AAV_ITGs enhanced transduction in skeletal muscle following systematic administration

AAV_ITGs, together with AAV9 and AAV9rh74, were administrated systematically via intravenous injection (transgene: CMV_GFP-Luciferase, dose: 1E13 vg/kg, age at injection: 6 weeks, n = 4) in C57Bl6 mice to examine their biodistribution 3 weeks post-injection (**Fig. 3A**).

In agreement with a previous study, AAV9rh74 slightly reduces transduction in skeletal muscle compared to AAV9 but accumulates much less in the liver (**Fig. 3B-D**). Thanks to the liver-detargeting capsid and in accordance with the fact that αVβ6 is weakly expressed in the liver, we expected poor entry into the liver for designed AAV_ITGs. Indeed, AAV_ITGs is strongly detargeted from the liver, both at VCN and mRNA levels, even further than the parental capsid (**Fig. 3C-D**). In contrast, enhanced transduction was observed in all skeletal muscles that were tested, including the tibialis anterior (TA), quadriceps (Qua) and diaphragm (Dia) (**Fig. 3B-D**). The two AAV_ITGs both showed a substantial increase in VCN and luciferase activity compared to both AAV9 and AAV9rh74. Similar to the results obtained in *in vitro* models, AAV9rh74_4um9 is the best transducer among the two AAV_ITGs. Compared to AAV9, the variant 9rh74_4um9 significantly increased VCN 5.31/7.21/2.48-fold and increased luciferase activity 15.2/13.2/23.57-fold in Qua, TA, and Dia ($p < 0.05$), respectively. Compared to the original backbone AAV9rh74, this variant even magnified the difference by increasing VCN 5.53/2.85/7.69-fold and increasing luciferase activity 152.35/106.68/60.43-fold ($p < 0.05$). Furthermore, AAV9rh74_4um9, but not AAV9rh74_5ffo, significantly increased transduction in the heart ($FC_{VCN}=4.15$, $FC_{LUC}=15.43$, $p < 0.05$). All AAVs that were tested showed poor delivery and transgene expression in the lungs and kidneys. No alteration of TGFβ and integrin signaling was observed at one-month post-injection in all AAVs being tested (**Fig S2F-G**). Overall, these data indicate that AAV_ITGs, especially the 9rh74_4um9 variant, are strongly liver-detargeted and exhibit enhanced tropism towards skeletal and cardiac muscles.

5. AAV9rh74_4um9 transduced skeletal muscle similarly, but detargeted the liver more strongly than other myotropic AAVs

Several engineered myotropic AAVs (mAAVs), including AAVMYO [15], MYOAAV-1A and – 2A [17], have demonstrated superior efficacy for *in vivo* delivery of muscle compared to natural AAVs. To evaluate the properties of these AAVs compared to ours, we performed *in vitro* and *in vivo* experiments. Viral preparations were produced using the same reporter transgene (CMV_GFP-Luc). All mAAVs were well-produced in 400ml suspension, with higher titers than AAV9rh74. However, MYOAAV productivity was significantly lower than 9rh74_ITGs and MYOAAVs (**Fig S3A**). Since all investigated mAAVs shared a common integrin-targeting RGD motif, these AAVs were then evaluated for their transduction via integrin complexes in myotubes and in cell lines where integrin complexes were stably overexpressed by the PiggyBac system. In 293_αVβ6 cells as well as in hMT, where αVβ6 is highly expressed, AAV9rh74_4um9 showed the highest transduction among the tested myotropic AAVs, with the sole exception that luciferase activity of MYOAAV2A was higher in hMT (**Fig S3B-C**). We also tested AAV transduction efficiency in two other cell lines, 293_WT, where αVβ6 expression is low, and 293_α7β1 that stably overexpresses a non-RGD-targeting α7β1 integrin. In both conditions, MYOAAV2A and AAV9rh74_4um9 showed the highest transduction (**Fig S3D-E**). These results suggest that, as intended with the rational design, AAV9rh74_4um9 uses αVβ6 more preferentially for cellular transduction than others, yet it can also efficiently use other integrin(s) similar to MYOAAV2A.

Following *in vivo* injection in the same setting as described above (6-week-old WT mice, dose: 1E13 vg/kg, n = 4), the three mAAVs and 9rh74_4um9 all showed strong liver-detargeting, high enrichment in both skeletal and cardiac muscles, and negligible transduction levels in other organs that were tested (kidneys, lungs, and brain) (**Fig. 3G-H**). No significant difference was observed in either VCN or luciferase activity between all three mAAVs and 9rh74_4um9 in the skeletal muscles that were tested. In heart muscle, MYOAAV2A showed a significant increase in VCN compared to other myotropic vectors, but no difference in luciferase activity, in agreement with the original observation [17]. The most striking difference is the level of liver-detargeting between these vectors. The VCN for 9rh74_4um9 in liver is 3.34/22.05/13.85 times lower than for AAVMYO ($p = 0.0022$), MYOAAV-1A ($p = 0.0013$) and – 2A ($p = 0.033$), respectively (**Fig. 3G**), and is therefore the only vector that accumulates less in liver than skeletal muscles (**Fig S3F-G**). These data indicate higher muscle specificity for the 9rh74_4um9 variant compared to other myotropic vectors that have been investigated to date.

In summary, the 9rh74_4um9 variant, hereafter referred to as LICA1 (linked-integrin-complex AAV), consistently showed enhanced transduction and strongest liver-detargeting. Therefore, we then attempted to evaluate LICA1 as a delivery vector for muscular dystrophies, in comparison with AAV9. Two different setups will be investigated: the transfer of microdystrophin (μDys) – an incomplete transgene - in mdx, a mild mouse model of Duchenne muscular dystrophy (DMD) and of the full-length human α-sarcoglycan (SGCA) in a severe mouse model of limb-girdle muscular dystrophy R3 (LGMD-R3).

6. Low-dose LICA1-μDys gene transfer is effective in specifically overexpressing microdystrophin in dystrophic muscle but not sufficient to fully correct the underlying pathology

DMD is caused by mutations in the DMD gene, which encodes for dystrophin protein – a key player in the dystrophin-glycoprotein complex (DGC), which is critical for the structural stability of skeletal muscle fibers [39]. Lack of dystrophin can result in progressive loss of muscle function, respiratory defects, and cardiomyopathy. The most commonly used DMD animal model is the mdx mouse, with a lifespan reduced by 25%, milder clinical symptoms than those seen in human patients, with the exception of the diaphragm muscle [40]. Among many therapeutic strategies to restore dystrophin expression, high-dose AAV-based gene transfer of shortened functional forms of the dystrophin ORF provided excellent results in animal models, but unsatisfactory conflicting data in current clinical trials [6]. Severe toxicities, even patient death, have been reported from these trials (NCT03368742, NCT04281485), assumed to be related to the dose of ≥ 1E14 vg/kg. We therefore explored the possibility of low-dose µDys gene transfer [41] in mdx mice using LICA1 in comparison to AAV9 (**Fig S4A**, age at injection: 4 weeks, dose: 5E12 vg/kg, treatment duration: 4 weeks, n = 5). Three muscles with increasing levels of severity – TA, Qua, and Dia – were used to study AAV transduction and treatment efficacy.

LICA1 showed better µDys gene transfer than AAV9 in this model. LICA1-treated mice exhibited a significantly higher VCN in all 3 muscles that were tested, 1.85/2.02/1.07 times higher in TA ($p < 0.0001$), Qua ($p < 0.0001$), and Dia ($p = 0.020$), respectively (**Fig. 4A**). RNA levels indicated even greater differences and were 4.56–7.57 times higher in the LICA1-treated group (**Fig. 4B**; TA: FC = 4.56, $p < 0.0001$; Qua: FC = 5.46, $p = 0.0001$; Dia: 7.57, $p = 0.05$). Consequently, LICA1 can transduce almost 100% in TA and Qua, and 49.98% in Dia, while substantially lower numbers were seen in AAV9-treated muscles, at 73.22% ($p = 0.0001$), 57.8% ($p < 0.0001$), 10.34% ($p < 0.0001$) in TA, Qua, Dia, respectively (**Fig. 4C, Fig S4B**). Furthermore, while infection levels and expression of the transgene in liver were high for the AAV9 vector (despite the use of muscle-specific promoter), the VCN and mRNA levels in LICA1-treated liver were extremely low (**Fig. 4A-B**, $FC_{VCN:AAV9/LICA1}=36.8$, $p = 0.0002$; $FC_{mRNA:AAV9/LICA1}=64.7$, $p < 0.0001$). These data again confirmed the transduction efficiency and specificity towards skeletal muscle for the LICA1 vector, even with low-dose treatment.

The histological features and muscle functionality after AAV treatment were restored accordingly. The centronucleation index (percentage of centronucleated fibers) – an indicator of the regeneration/degeneration process – did not change with AAV9 (except in TA) but was significantly reduced upon LICA1 treatment (reduction of 21.68%, 19.05%, 22.88% in TA, Qua, Dia, respectively) (**Fig. 4D, Fig S4C**). Similarly, the fibrosis level in two severely affected muscles, Qua and Dia, only exhibited a significant reduction with LICA1, but not AAV9 (**Fig. 4E, Fig S4D**). The serum biomarker MYOM3 level, an indicator of muscle damage [42], showed a reduction for both AAV treatments, with a considerable further reduction seen in the LICA1-treated group (**Fig. 4F**, $FC_{AAV9/KO}=0.75$, $FC_{LICA/KO}=0.43$, $p_{AAV9-LICA1}>0.0001$). More importantly, AAV9 treatment did not affect any muscle functionality being tested (**Fig. 4G-I**), while significant improvements with LICA1-µDys treatment were observed in escape test – a measure of global force (**Fig. 4G**, $FC_{LICA1/mdx}=1.19$, $p_{LICA1/mdx}=0.02$) and *in situ* TA mechanical force measurement (**Fig. 4H**, $FC_{LICA1/mdx}=1.14$, $p_{LICA1/mdx}=0.0006$). However, none of the treatment normalized

to the WT functional levels. These data indicate that LICA1 is better than AAV9 at restoring dystrophic histological features and muscle functions.

We also investigated the molecular alteration in Qua upon AAV treatment using RNA-seq. On the two first principal components (PCs) of the PCA, a clear distinction between four transcriptome groups (WT, mdx, AAV9, LICA1) was observed, while LICA1-treated muscles were clustered closer to the WTs than others (**Fig S4E**). To our surprise, despite excellent transgene expression by LICA1, global transcriptomic restoration was relatively modest (**Fig. 4K**). Nevertheless, a substantial improvement can still be seen for LICA1 compared to AAV9. Among 4216 down- and 4501 upregulated differentially expressed genes (DEGs) identified in mdx muscle, 1515 (35.9%) and 1728 (38.4%) were restored by AAV9, while LICA1 was able to correct 1736 (41.2%) and 1980 (44.0%), respectively (**Fig. 4L-M**). In addition, a greater number of genes were either not or insufficiently corrected by AAV9 than by LICA1 (**Fig. 4N**). A total of 2572 genes were downregulated (61.0%) and 2620 (58.2%) incompletely restored, while significantly lower numbers were seen for LICA, with 2094 (49.67%) down- and 2019 (44.86%) upregulated. Interestingly, some known dysregulated pathways, including α- and Ɣ-interferon responses and oxidative phosphorylation, were significantly better normalized by LICA1 than by AAV9 (**Fig S4F**).

In summary, at 5E12 vg/kg, LICA1-μDys, but not AAV9, was efficient in transducing close to 100% myofibers, except in the diaphragm. This effective improvement in transduction can significantly reduce some dystrophic features in all muscles that were tested, yet restoration in the global transcriptome remains modest. However, greater improvements in functional, histological, and transcriptomic restoration were achieved with LICA1 compared to AAV9.

7. Low-dose LICA1-SGCA treatment restored the muscle functionality, dystrophic phenotypes, and transcriptomic dysregulation in a severe SGCA mouse model.

LGMDR3 is caused by mutations in the SGCA gene [43] – another component of the DGC complex. Defects in the SGCA protein therefore lead to muscle weakness and wasting. A LGMDR3 mouse model has been established, which closely represents patient's clinical phenotypes [44]. Similar to the setting in mdx mice, low-dose AAV treatment with 5E12 vg/kg was investigated in this mouse model. AAV9 or LICA1 encoding human SGCA (hSGCA) under control of a muscle-specific human Acta1 promoter were injected into 4-week-old SGCA-KO mice (**Fig. 5A**). Analysis was performed 4 weeks post-treatment.

In all three muscles that were tested, TA, Qua, Dia (in order of increasing severity), transduction in various measures, VCN, mRNA level, and percentage of SGCA + myofibers, was significantly greater in the LICA1-treated group than for AAV9 (**Fig. 5B-D, Fig S5A**). Of note is the fact that the differences in transduction efficacy (%SGCA + myofibers) between LICA1 and AAV9 are greater in more severely affected muscles (**Fig. 5D**). At such a low dose, AAV9 was able to transduce > 80% myofibers in TA while LICA1 can reach close to 100% ($p < 0.0001$). While LICA1 still transduced almost 100% of fibers in Qua (the muscle affected with intermediate severity), only 58.1% fibers were transduced by AAV9 on average ($p < 0.0001$).

In the most severely affected muscle, Dia, both vectors displayed reduced efficiency; however, LICA1 continued to demonstrate much better transduction (μ_{AAV9} = 22.1%, μ_{LICA1} = 59.5%, $p < 0.0001$).

The differences in transgene delivery and expression positively correlated with levels of histological and functional restoration. Different dystrophic histological features, including percentage of centronucleated fibers (**Fig. 5E, Fig S5B**), percentage of fibrosis area (**Fig. 5F, Fig S5C**), and fiber size distribution (**Fig. 5G**), were all significantly better normalized by LICA1 than AAV9, especially in more severely affected muscles. Importantly, no significant improvement was observed in the AAV9-treated group in centronucleation index and fibrosis level in Dia, while LICA1 reduced these parameters by half (**Fig. 5E-F**). Fiber sizes were also restored to near-WT distribution by LICA1 in this muscle (**Fig. 5G**). No difference in body weight was seen between groups with or without AAV treatment (**Fig S5D**). At the functional level, however, the escape test – a measure of global force - showed a significant increase in AAV9-treated mice (FC = 1.42, p = 0.0072) and was even higher in LICA1-treated group (FC = 1.72, $p < 0.0001$) (**Fig. 5H**). On the other hand, *in situ* TA mechanical forces were both improved in the two AAV groups at similar levels (**Fig. 5I**), possibly due to > 80% transduction rate by both vectors. Similar to the global force, the serum MYOM3 level was greatly reduced in the LICA1-treated group but not for AAV9, indicating less muscle damage (**Fig. 5K**). No difference was seen in the anti-capsid antibody between the two AAV treatments (**Fig S5E**). These results indicate that better and significant functional and histological restoration in the LICA1-treated mice was achieved, even at low-dose treatment, thanks to superior transduction efficacy.

We further investigated the molecular alterations following AAV treatment by transcriptomic profiling of the quadriceps muscle. The first principal component (PCs) of the PCA was able to separate a group including WT and LICA1 with a group including SGCA-KO and AAV9, suggesting close proximity between elements within these 2 groups (**Fig S5F**). A heatmap of all 8591 significant DEGs (4035 downregulated and 4556 upregulated) further highlighted the restorative effect of LICA1 on gene expression levels (**Fig. 5L**). LICA1-treated muscles, in particular, demonstrated a significant correction of 69.9% (2821/4035) and 66.5% (3028/4556) of down- and upregulated DEGs, respectively, compared to 12.4% (500/4035) and 9.21% (420/4556) corrected by AAV9 treatment (**Fig. 5M-N**). Conversely, not all DEGs were significantly restored or returned to WT levels. The number of such transcripts in AAV9-treated muscles was much higher than in the LICA1-treated group (**Fig. 5O**): 2541 (63.0%) downregulated DEGs and 3045 (66.8%) upregulated DEGs for AAV9, with only 483 (12.0%) downregulated DEGs and 1038 (22.8%) upregulated DEGs in the LICA1-treated group. These data illustrate that low-dose LICA1 treatment can effectively normalize the majority of the dysregulated transcriptome and is much more efficient in correcting gene expression dysregulation than AAV9 at the same dose.

In summary, low-dose (5E12 vg/kg) AAV gene transfer using LICA1 in the LGMDR3 mouse model is effective in restoring muscle function, dystrophic histology, and the dysregulated transcriptome. The efficacy was much greater than for AAV9 at the same dose due to enhanced transduction.

DISCUSSION

Given the severe complications observed with very high dose AAV treatment, lowering the dose by increasing vector specificity via capsid modification is one way to address these issues. This study investigated the possibility of altering AAV tropism towards skeletal muscle by targeting integrin. We designed an AAV as a αVβ6 binder, which resulted in a novel myotropic AAV variant, namely LICA1. LICA1 showed greatly enhanced transduction in skeletal muscle in WT and two MD mouse models. Consequently, by improving the delivery of therapeutic transgenes (hSGCA and μDys) in these MD mouse models, LICA1 was able to correct dystrophic phenotypes, global transcriptional dysregulations and significantly restore muscle function.

AAV capsid sequence design method that ensures high AAV production

AAV tropism is commonly altered by inserting a small peptide into the VR4 or VR8 loop without any sequence constraints. Since no consideration regarding AAV capsid stability is included in this method, the resulting AAV can suffer from instability, reduced productivity, and increased AAV genome fragmentation [17, 45](ASGCT 2023). In the current study, a physics-based protein sequence design method was used to graft the binding motifs from TGFβ-1 and − 3 into the VR4 loop of the hybrid capsid AAV9rh74. The major differences to the classical peptide insertion method are that the entire VR4 loop was modified to include a new binding motif and the amino acids around this motif (linkers) were selected to minimize the potential energy. Low-energy sequences ensure the stability and intended folding of the designed proteins, presumably leading to improved stability of the AAV particle [38]. Six AAVs designed using this method were tested experimentally and all showed better productivity than their parent, Cap9rh74, and similar levels to well-produced AAV9. This suggests that low Rosetta energy correlates with high stability of capsid protein, and thereby high AAV production.

Integrin αVβ6 as a myotropic AAV receptor for skeletal muscle

Virus-host interaction is the foundation for improved viral vectors, yet skeletal muscle receptors that allow effective AAV transduction are poorly defined. However, top hits from two independent studies with different screening schemes identified myotropic AAVs with a common RGD motif, [15, 17, 19]. In addition, it has previously been described that integrin functions as cellular receptor for natural AAV [23, 24]. Coincident with our screening for possible integrin receptor, only αVβ6 is highly expressed and enriched in skeletal muscle (**Fig S1)**. By including αVβ6 binding motifs, AAV_ITGs efficiently utilized αVβ6 for cellular infection. Enhanced transduction was observed in conditions with high (either ectopic or natural) αVβ6 expression, including human differentiated myotubes and murine skeletal muscles of WT and two other MD mouse models. In most cases, the improved transduction was evident at the VCN level, indicating better cell entry via αVβ6 binding.

In addition, we conducted a study comparing LICA1 and three other published myotropic AAVs. No significant differences in skeletal muscle transduction were observed on either VCN or transgene expression levels. However, the liver infection rate was significantly lower with LICA1 compared to the other mAAVs, presumably due to the use of a liver-detargeted backbone and the low expression level of

αVβ6 in liver. As a result, the LICA1 vector exhibited the highest muscle/liver transduction ratio among all AAVs tested, suggesting increased specificity towards skeletal muscle. This finding highlights the importance of selecting an appropriate targeting receptor for rational design and further supports αVβ6 as a promising candidate for targeting skeletal muscle.

LICA1 is a potential vector for muscular diseases

AAV gene therapy in muscle diseases typically requires very high doses (≥ 1E14 vg/kg) for functional benefits [41, 46], yet can result in severe and even fatal adverse events [7]. In this study, we explored low dose (5E12 vg/kg) treatment using the LICA1 vector in two MD mouse models, DMD and LGMDR3. Of note is that this dose is at least 20 times lower than the doses currently used in clinical trials for neuromuscular diseases [3]. In both models, LICA1 was significantly better than AAV9 in delivering and expressing therapeutic transgenes, consequently restoring better histological dystrophic phenotypes. In TA and Qua, LICA1 was able to transduce more than 80% of fibers. It was still a challenge to effectively transduce diaphragm muscle at this dose, yet more than 50% of Dia fibers were positive for transgene expression with LICA1 in both models while AAV9 transduced very poorly. This improvement in transgene expression translates directly into improved histological restoration, including centronucleation index and fibrosis level. In particular, with only more than 50% successfully transduced fibers, LICA1 was able to reduce diaphragm fibrosis by 42.8–47.0% (mdx and SGCA$^{-/-}$ models respectively), whereas no change was seen in AAV9-treated groups. The biomarker for muscle damage level, MYOM3, was reduced by 57.5–67.2% (mdx and SGCA$^{-/-}$ models respectively) by LICA1 and significantly greater than AAV9. Similarly, global muscle force was significantly restored to a higher level with LICA1 than with AAV9 in SGCA-KO mice. These data confirmed superior muscle transduction by LICA1 and resulting therapeutic benefits were obtained even at low-dose treatment in two MD models.

However, treatment efficacy varies between two disease models at molecular levels. We profiled transcriptomic changes in Qua following AAV treatment in both MD models. Despite similar transduction efficiency of LICA1 in the two models, restoration of dystrophic transcriptional changes in SGCA-KO was significantly greater. It is noteworthy that μDys is an incomplete form of dystrophin. The μDys used in the present study lacks several functional domains, including multiple spectrin-like repeats that bind to nNOS, F-actin, sarcomeric lipid and microtubules, and a dystrobrevin- and syntrophin-binding C-terminus [41]. This might explain the inadequate efficacy in restoring global gene expression in μDys gene therapy trials, in spite of highly effective gene transfer. Similarly, despite excellent functional restoration by microdystrophin gene transfer in various animal models, outcomes from these clinical trials are unsatisfactory [6]. Therefore, careful assessment of molecular restoration should be included for evaluating gene therapy efficacy.

In summary, this study presents an alternative computational method that aids rational AAV design and ensures high-production AAV variants. The proof-of-concept design targeting skeletal muscle resulted in a high-productivity myotropic AAV, thereby effectively delivering therapeutic transgenes and restoring dystrophic phenotypes in two MD mouse models at a low dose. This work contributes to the ongoing

efforts to reduce AAV treatment doses and further advance AAV engineering, paving the way for more effective and accessible gene therapies in the future.

MATERIALS AND METHODS

Study Design

The primary objective of the study was to design a novel myotropic AAV capsid with a high production yield by using a computationally rational design. The secondary aim was to investigate the possibility of low-dose AAV treatment using a designed AAV in animal models of muscular dystrophies, which typically require an alarmingly high dose (≥ 1E14 vg/kg). We used publicly available datasets to identify possible receptors for skeletal muscle and protein design tools to engineer AAV capsid protein. Resulting variants were characterized for their productivity and transduction efficiency in various *in vitro* cell lines and multiple mouse models. Experiments were performed at least three times, unless noted otherwise. The AAV injection and infection experiments were conducted in a nonblinded fashion. The blinding approach was used during dissection, histological validation, immunostaining analysis, *in vivo* functional tests, and biomarker analysis. No data were excluded. Details on experimental procedures are presented in **Supplementary Materials and Methods**.

Animal care and use

All animals were handled according to French and European guidelines for human care and the use of experimental animals. All procedures on animals were approved by the local ethics committee and the regulatory affairs of the French Ministry of Research (MESRI) under the numbers 2018-024-B #19736, 2022-004 #35896. C57Bl/6, B6Ros.Cg-Dmdmdx-4Cv/J mice were obtained from the Jackson Laboratory. A knockout mouse model of *α*-sarcoglycan was obtained from the Kevin Campbell laboratory (University of Iowa, USA) [44]. Mice were housed in a SPF barrier facility with 12-h light, 12-h dark cycles, and were provided with food and water *ad libitum*. Only male mice were used in the present study. Well-being and weights of the animals were monitored for the duration of the study. The animals were anesthetized with a mix of ketamine (100 mg/kg) and xylazine (10 mg/kg), or with isoflurane (4%) for blood samples. For AAV intravenous injections, a maximum volume of 150 µl containing AAV vectors was injected via the sinus route after the animals had been anesthetized with isoflurane. The AAV intravenous doses used in the present study were 5E12 or 1E13 vg/kg.

Cell culture and in vitro study

Adherent HEK293-T cells were maintained in the proliferating medium containing DMEM (Thermo Fisher Scientific), supplied with 10% fetal bovine serum and 1X gentamycin at 37ºC, 5% CO2. Human immortalized myoblasts (AB1190 cell line) were maintained in Skeletal Muscle Cell Growth Medium (PromoCell, C23060) and differentiated in Skeletal Muscle Differentiation Medium (PromoCell, C23061).

In vitro AAV infection was performed by directly adding AAV into culture medium at the dose of 1E9 or 1E10 vg per 24-well plate well. After 48h post-infection, cells were washed and subjected to VCN and gene expression analysis.

To inhibit AAV infection, AAVs were incubated with recombinant hITGAV-hITGB6 protein (Bio-Techne, 3817-AV-050) at 37°C for 30 minutes, at a concentration of 1µg protein per 5E9vg AAV before addition to the cells (1E4 vg per cell). The same condition treated with recombinant hSGCA protein served as a control for the comparison.

Statistical Analysis

Results are presented as mean ± SEM, unless noted otherwise. Significance of differences in multiple pairwise comparisons of more than two groups was determined by one-way ANOVA. The significance of differences in pairwise comparisons of multiple groups with multiple treatments was determined by two-way ANOVA. To account for multiple testing and control the false discovery rate (FDR) across the numerous pairwise comparisons, the Benjamini-Hochberg (BH) procedure was applied with an FDR threshold of 0.05. Statistical tests were performed using GraphPad Prism 9. Results were considered significant when p-values or adjusted p-values were less than 0.05.

DECLARATIONS

Acknowledgments: The authors are Genopole's members, first French biocluster dedicated to genetic, biotechnologies and biotherapies. We are grateful to the “Imaging and Cytometry Core Facility” and to the *in vivo* evaluation, services of Genethon for technical support, to Ile-de-France Region, to Conseil Départemental de l’Essonne (ASTRE), INSERM and GIP Genopole, Evry for the purchase of the equipment. We would like to acknowledge the technical help of Carolina Pacheco Algalan and Alejandro Arco Hierves. The Genotype-Tissue Expression (GTEx) Project was supported by the Common Fund of the Office of the Director of the National Institutes of Health, and by NCI, NHGRI, NHLBI, NIDA, NIMH, and NINDS.

Funding: This work was supported by the “Association Française contre les Myopathies” (AFM), and “Institut National de la Santé Et de la Recherche Médicale” (INSERM, FranceRelance N°221513A10).

Author contributions: The project was conceptualized by A.H.V. and I.R. A.H.V., L.S.P., and J.P. conducted experiments and performed data analysis. Funding supporting this project was obtained by I.R. A.H.V. and I.R. supervised the project. The manuscript was written by A.H.V. and I.R.

Competing interests: A.H.V. and I.R. are inventors on PCT application EP2023/065499 for the integration of RGDLxxL/I motif in AAV capsid for enhanced muscle transduction efficiency. I.R. is a part-time employee of Atamyo Therapeutics. The other authors declare that they have no competing interests.

Data and materials availability: All data associated with this study are present in the paper or the Supplementary Materials. All transcriptomic data will be deposited in the NCBI Sequence Read Archive

(SRA) upon publication. Processed data including differential gene expression analysis are available in data file S1 and S2. The plasmid constructs and reagents generated as part of this study are available under a material transfer agreement from the corresponding authors.

REFERENCES

1. Wang, D., Tai, P.W.L. & Gao, G. Adeno-associated virus vector as a platform for gene therapy delivery. *Nat Rev Drug Discov* **18**, 358-378 (2019).
2. Pupo, A. et al. AAV vectors: The Rubik's cube of human gene therapy. *Molecular therapy : the journal of the American Society of Gene Therapy* **30**, 3515-3541 (2022).
3. Crudele, J.M. & Chamberlain, J.S. AAV-based gene therapies for the muscular dystrophies. *Hum Mol Genet* **28**, R102-R107 (2019).
4. Duan, D. Systemic AAV Micro-dystrophin Gene Therapy for Duchenne Muscular Dystrophy. *Molecular therapy : the journal of the American Society of Gene Therapy* **26**, 2337-2356 (2018).
5. Mack, D.L. et al. Systemic AAV8-Mediated Gene Therapy Drives Whole-Body Correction of Myotubular Myopathy in Dogs. *Molecular therapy : the journal of the American Society of Gene Therapy* **25**, 839-854 (2017).
6. Mercuri, E., Bonnemann, C.G. & Muntoni, F. Muscular dystrophies. *Lancet* **394**, 2025-2038 (2019).
7. Ertl, H.C.J. Immunogenicity and toxicity of AAV gene therapy. *Front Immunol* **13**, 975803 (2022).
8. Verdera, H.C., Kuranda, K. & Mingozzi, F. AAV Vector Immunogenicity in Humans: A Long Journey to Successful Gene Transfer. *Molecular therapy : the journal of the American Society of Gene Therapy* **28**, 723-746 (2020).
9. High-dose AAV gene therapy deaths. *Nature biotechnology* **38**, 910 (2020).
10. Ogden, P.J., Kelsic, E.D., Sinai, S. & Church, G.M. Comprehensive AAV capsid fitness landscape reveals a viral gene and enables machine-guided design. *Science* **366**, 1139-1143 (2019).
11. DiMattia, M.A. et al. Structural insight into the unique properties of adeno-associated virus serotype 9. *Journal of virology* **86**, 6947-6958 (2012).
12. Li, C. & Samulski, R.J. Engineering adeno-associated virus vectors for gene therapy. *Nat Rev Genet* **21**, 255-272 (2020).
13. Tseng, Y.S. & Agbandje-McKenna, M. Mapping the AAV Capsid Host Antibody Response toward the Development of Second Generation Gene Delivery Vectors. *Front Immunol* **5**, 9 (2014).
14. Buning, H. & Srivastava, A. Capsid Modifications for Targeting and Improving the Efficacy of AAV Vectors. *Molecular therapy. Methods & clinical development* **12**, 248-265 (2019).
15. Weinmann, J. et al. Identification of a myotropic AAV by massively parallel in vivo evaluation of barcoded capsid variants. *Nature communications* **11**, 5432 (2020).
16. El Andari, J. et al. Semirational bioengineering of AAV vectors with increased potency and specificity for systemic gene therapy of muscle disorders. *Science advances* **8**, eabn4704 (2022).

17. Tabebordbar, M. et al. Directed evolution of a family of AAV capsid variants enabling potent muscle-directed gene delivery across species. *Cell* **184**, 4919-4938 e4922 (2021).
18. Ruoslahti, E. & Pierschbacher, M.D. Arg-Gly-Asp: a versatile cell recognition signal. *Cell* **44**, 517-518 (1986).
19. Bauer, A. et al. Molecular Signature of Astrocytes for Gene Delivery by the Synthetic Adeno-Associated Viral Vector rAAV9P1. *Adv Sci (Weinh)* **9**, e2104979 (2022).
20. Zolotukhin, S., Trivedi, P.D., Corti, M. & Byrne, B.J. Scratching the surface of RGD-directed AAV capsid engineering. *Molecular therapy : the journal of the American Society of Gene Therapy* **29**, 3099-3100 (2021).
21. Hynes, R.O. Integrins: a family of cell surface receptors. *Cell* **48**, 549-554 (1987).
22. Hussein, H.A. et al. Beyond RGD: virus interactions with integrins. *Arch Virol* **160**, 2669-2681 (2015).
23. Asokan, A., Hamra, J.B., Govindasamy, L., Agbandje-McKenna, M. & Samulski, R.J. Adeno-associated virus type 2 contains an integrin alpha5beta1 binding domain essential for viral cell entry. *Journal of virology* **80**, 8961-8969 (2006).
24. Summerford, C., Bartlett, J.S. & Samulski, R.J. AlphaVbeta5 integrin: a co-receptor for adeno-associated virus type 2 infection. *Nat Med* **5**, 78-82 (1999).
25. Stewart, P.L. & Nemerow, G.R. Cell integrins: commonly used receptors for diverse viral pathogens. *Trends Microbiol* **15**, 500-507 (2007).
26. Strauch, E.M. et al. Computational design of trimeric influenza-neutralizing proteins targeting the hemagglutinin receptor binding site. *Nature biotechnology* **35**, 667-671 (2017).
27. Cao, L. et al. Design of protein-binding proteins from the target structure alone. *Nature* **605**, 551-560 (2022).
28. Ruoslahti, E. RGD and other recognition sequences for integrins. *Annual review of cell and developmental biology* **12**, 697-715 (1996).
29. Chemello, F. et al. Degenerative and regenerative pathways underlying Duchenne muscular dystrophy revealed by single-nucleus RNA sequencing. *Proceedings of the National Academy of Sciences of the United States of America* **117**, 29691-29701 (2020).
30. Pang, X. et al. Targeting integrin pathways: mechanisms and advances in therapy. *Signal Transduct Target Ther* **8**, 1 (2023).
31. Shen, X., Storm, T. & Kay, M.A. Characterization of the relationship of AAV capsid domain swapping to liver transduction efficiency. *Molecular therapy : the journal of the American Society of Gene Therapy* **15**, 1955-1962 (2007).
32. Ballon, D.J. et al. Quantitative Whole-Body Imaging of I-124-Labeled Adeno-Associated Viral Vector Biodistribution in Nonhuman Primates. *Human gene therapy* **31**, 1237-1259 (2020).
33. Jumper, J. et al. Highly accurate protein structure prediction with AlphaFold. *Nature* **596**, 583-589 (2021).

34. Mirdita, M. et al. ColabFold: making protein folding accessible to all. *Nature methods* **19**, 679-682 (2022).
35. Dong, X. et al. Force interacts with macromolecular structure in activation of TGF-beta. *Nature* **542**, 55-59 (2017).
36. Dong, X., Hudson, N.E., Lu, C. & Springer, T.A. Structural determinants of integrin beta-subunit specificity for latent TGF-beta. *Nature structural & molecular biology* **21**, 1091-1096 (2014).
37. Huang, P.S. et al. RosettaRemodel: a generalized framework for flexible backbone protein design. *PloS one* **6**, e24109 (2011).
38. Alford, R.F. et al. The Rosetta All-Atom Energy Function for Macromolecular Modeling and Design. *Journal of chemical theory and computation* **13**, 3031-3048 (2017).
39. Duan, D., Goemans, N., Takeda, S., Mercuri, E. & Aartsma-Rus, A. Duchenne muscular dystrophy. *Nat Rev Dis Primers* **7**, 13 (2021).
40. Stedman, H.H. et al. The mdx mouse diaphragm reproduces the degenerative changes of Duchenne muscular dystrophy. *Nature* **352**, 536-539 (1991).
41. Bourg, N. et al. Co-Administration of Simvastatin Does Not Potentiate the Benefit of Gene Therapy in the mdx Mouse Model for Duchenne Muscular Dystrophy. *Int J Mol Sci* **23** (2022).
42. Rouillon, J. et al. Serum proteomic profiling reveals fragments of MYOM3 as potential biomarkers for monitoring the outcome of therapeutic interventions in muscular dystrophies. *Hum Mol Genet* **24**, 4916-4932 (2015).
43. Eymard, B. et al. Primary adhalinopathy (alpha-sarcoglycanopathy): clinical, pathologic, and genetic correlation in 20 patients with autosomal recessive muscular dystrophy. *Neurology* **48**, 1227-1234 (1997).
44. Duclos, F. et al. Progressive muscular dystrophy in alpha-sarcoglycan-deficient mice. *The Journal of cell biology* **142**, 1461-1471 (1998).
45. Bryant, D.H. et al. Deep diversification of an AAV capsid protein by machine learning. *Nature biotechnology* **39**, 691-696 (2021).
46. Israeli, D. et al. An AAV-SGCG Dose-Response Study in a gamma-Sarcoglycanopathy Mouse Model in the Context of Mechanical Stress. *Molecular therapy. Methods & clinical development* **13**, 494-502 (2019).

Figures

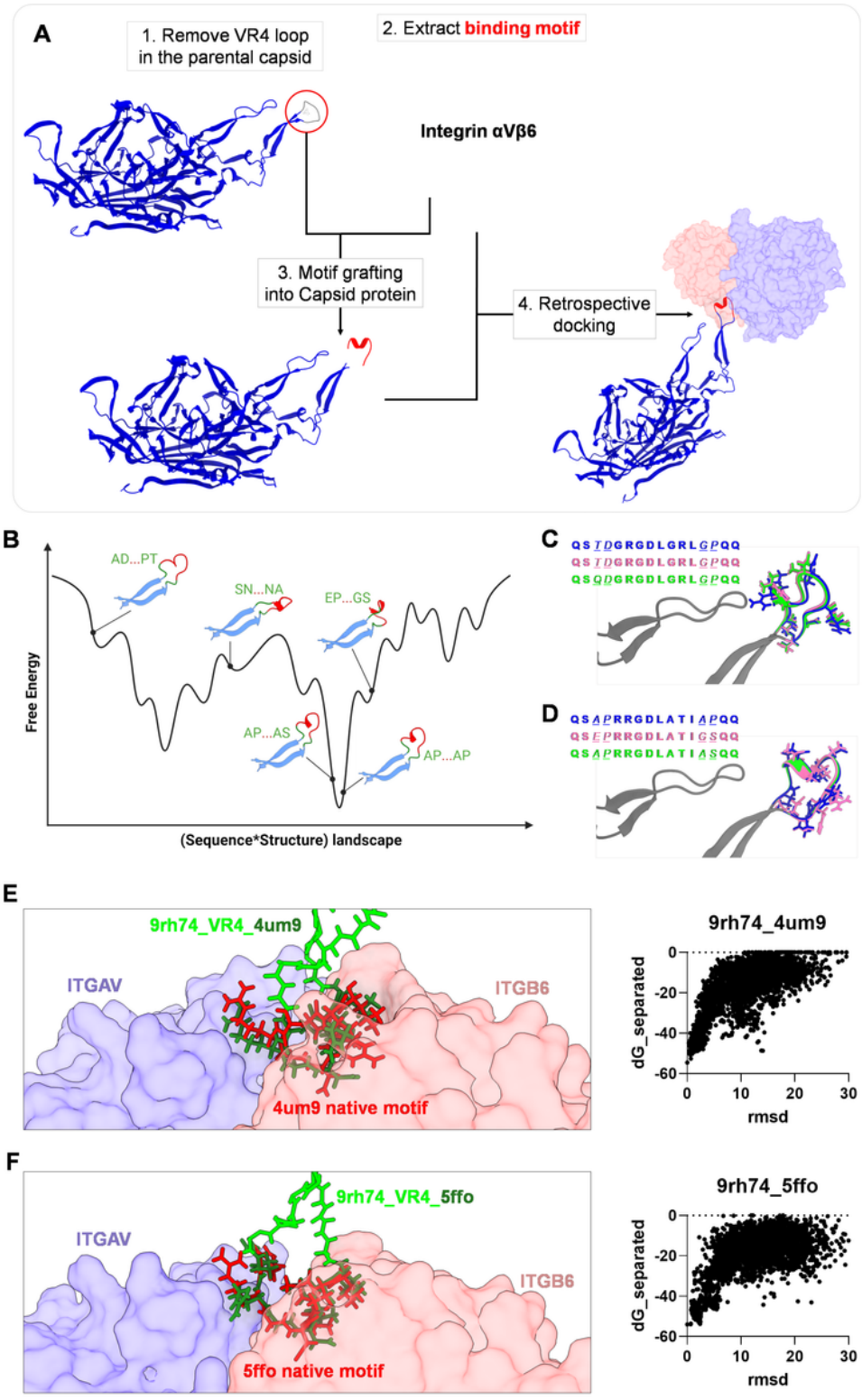

Figure 1

Computational rational AAV capsid design to bind to αVβ6 integrin

A. Overview of the design pipeline, including three steps: 1. Capsid 3D structures were obtained either from the PDB database or predicted by AlphaFold2. 2. The capsid VR4 loop was completely replaced by integrating the binding motif, which was extracted from receptor's natural binder, using RosettaRemodel

protocol. 3. Top scored designs from the previous grafting step were docked onto the intended receptor *in silico* to verify the binding potential of the designed capsid. **B**. An illustration of the sampling for low-energy sequence-structure pairs during motif-grafting process. Capsid VR4 after removing the loop was colored in blue, extracted binding motif was colored in red. The sampled linkers and sequences (**Fig. S1F**) were labeled in green. **C-D**. The three lowest energy designs after grafting TGFβ3 (**C**) and TGFβ1 (**D**) into the capsid VR4. All top designs showed convergence in structures and sequences, suggesting sampling approached the global optimum. **E-F**. Retrospective docking of motif-grafted capsids (**E**. Cap9rh74_4um9 and **F**. Cap9rh74_5ffo) onto the αVβ6 structure. The left panels are illustrations of the structures with the lowest energy at the interface of capsid and integrin proteins (dG_separated: difference in free energy of two proteins). Both two newly designed VR4s (colored in green) were predicted to bind to the αVβ6 complex at very similar positions to natural binding motifs (colored in red). The right panels are scatter plots of dG_separated energy versus root-mean-square deviation (RMSD) from the lowest energy structure of all sampled docking positions.

Fig. 2

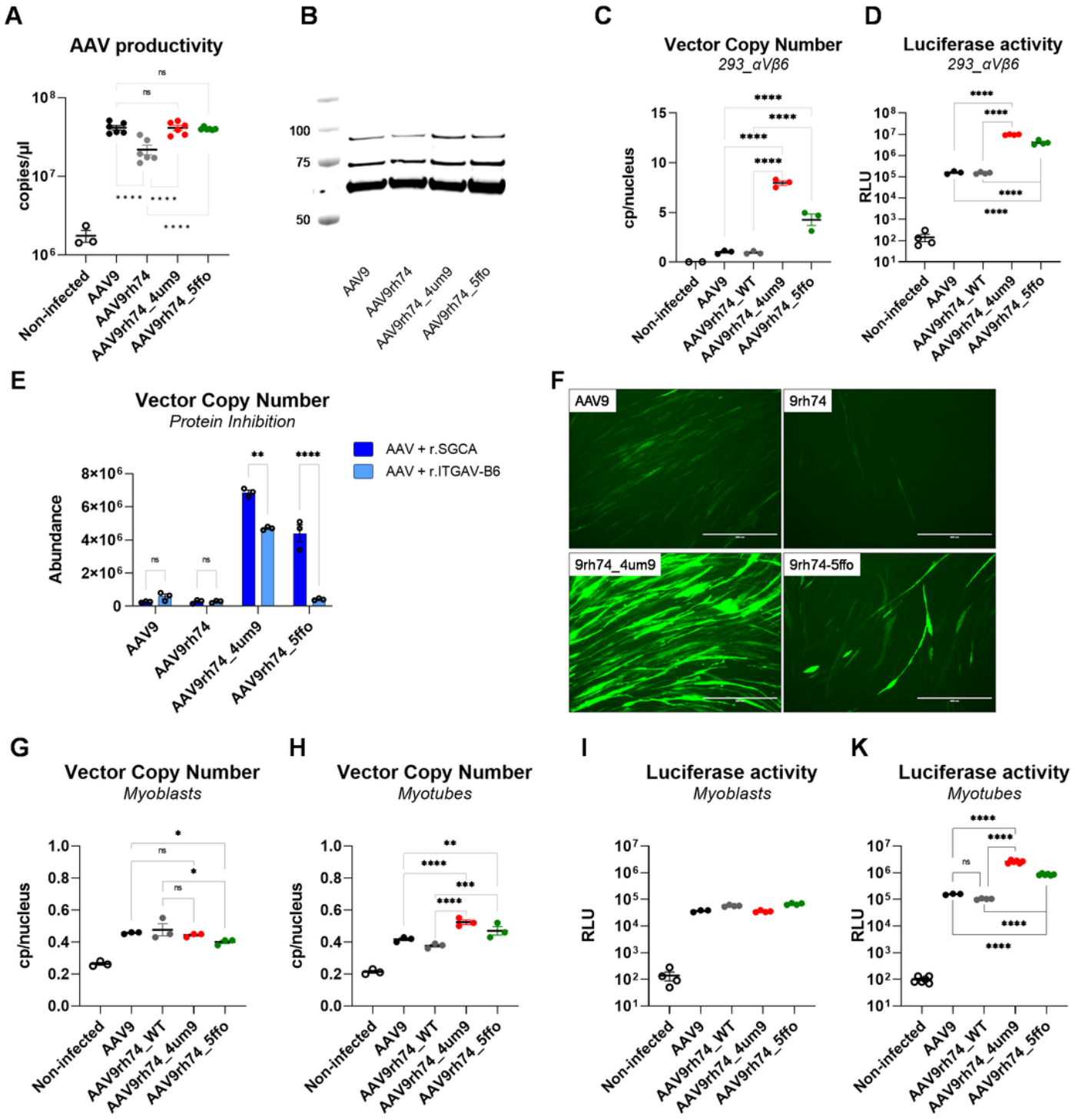

Figure 2

Designed AAV_ITGs were well-produced and improved transduction via αVβ6 binding.

A. AAV titers of different AAV variants in bulked small-scale production in suspension three-day post-triple-transfection (2ml production, n=6, one-way ANOVA). **B**. Western blot of VP proteins from purified AAVs showed similar VP ratios for designed AAV_ITGs capsids compared to AAV9 and AAV9rh74,

suggesting successful capsid assembly. **C-D**. VCN (**C**) and luciferase activity (**D**) of 293_αVβ6 after AAV infection (n=3-4, one-way ANOVA). Both the two designed AAV_ITGs showed enhanced VCN and luciferase activities compared to AAV9rh74 and AAV9. **E**. Inhibition of cell entry of designed AAV_ITGs, but not for AAV9 or AAV9rh74, in 293_αVβ6 cells by αVβ6 recombinant protein. AAVs were preincubated with αVβ6 recombinant protein (r.ITGAV-B6) for 30 minutes at 37°C before infection (n=3, two-way ANOVA). SGCA recombinant protein (r.SGCA) was used as the control. **F-K**. Enhanced transduction of AAV_ITGs in *in vitro* human differentiated myotubes, but not in myoblasts. **F**. Representative images of the GFP signal of myotubes 48 hours post-infection (scale bar: 400μm). **G-K**. VCN and luciferase activities of AAV_ITGs in comparison with AAV9 and AAV9rh74 in myoblasts (**G,I**) and myotubes (**H,K**) (n=3-4, one-way ANOVA).

Fig. 3

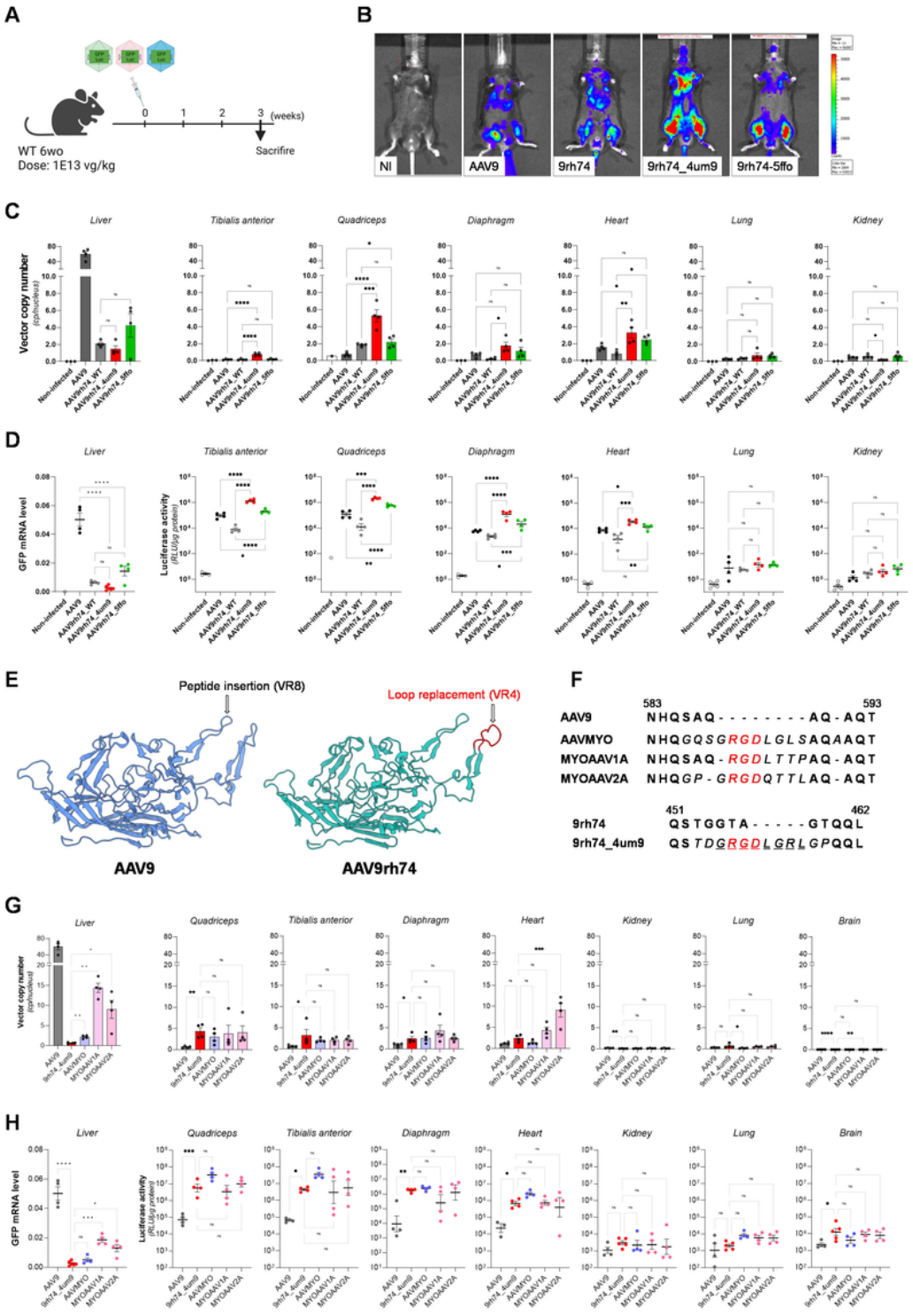

Figure 3

Designed AAV_ITGs showed enhanced transduction in skeletal and cardiac muscles while strongly liver-detargeted *in vivo*.

A. Scheme of *in vivo* experiment. AAVs (CMV_GFP-Luciferase) were injected intravenously into 6wo C57BL6 mice (n=4) at the dose of 1E13 vg/kg. **B**. Representative images of the bioluminescence signal

20 days post-infection. **C-D**. VCN (**C**) and gene expression (**D**) (GFP mRNA level in the liver and luciferase activity in other organs) for different AAVs in liver, skeletal muscles, heart, lung, and kidney (n=4, one-way ANOVA). Both designed AAV_ITGs strongly detargeted from the liver compared to AAV9, while they significantly improved VCN and luciferase activities over AAV9rh74 (and AAV9 with AAV9rh74_4um9 variant) in skeletal and cardiac muscles, and were detected and expressed at low levels in lung and kidney. **E-H**. Comparison of the AAV9rh74_4um9 variant with other public myotropic AAVs (mAAVs) [15, 17]. **E**. Illustration of the differences between mAAVs and AAV9rh74_4um9 at modification sites in capsid protein and modification methods. **F**. The VR8 loop sequences of mAAVs compared to VR8 of their backbone AAV9, and VR4 of AAV9rh74_4um9 compared to VR4 of AAV9rh74. **G-H**. VCN (**G**) and gene expression (**H**) (GFP mRNA level in liver and luciferase activity in other organs) of different AAVs in liver, skeletal muscles, heart, lung, kidney, and brain (n=4, one-way ANOVA). AAV9rh74_4um9 showed similar VCN and gene expression in skeletal muscle to other mAAVs, while being significantly more strongly detargeted from the liver.

Fig. 4

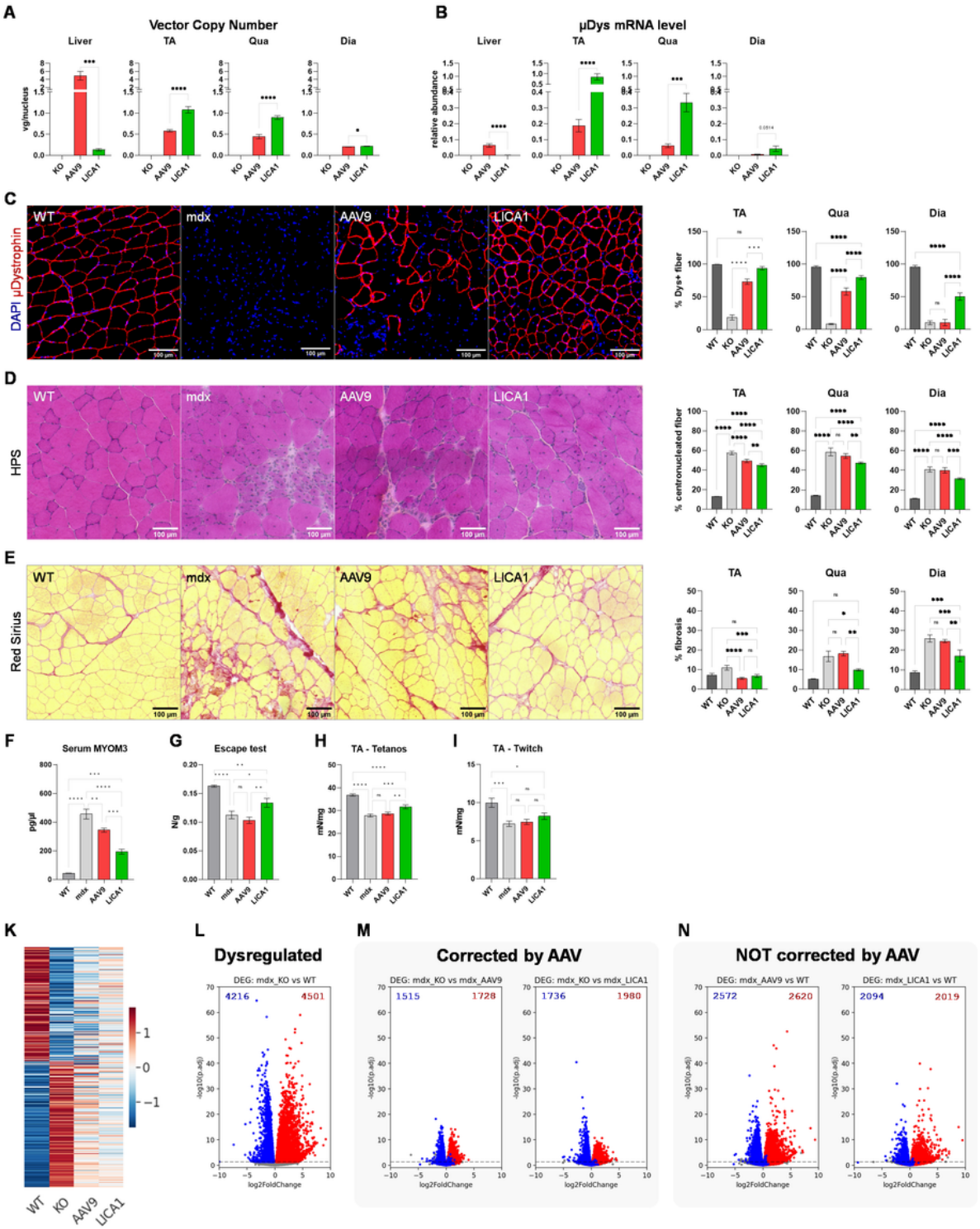

Figure 4

Low-dose gene transfer by LICA1 was more effective and better at restoring dystrophic phenotypes than AAV9 in the DMD mouse model.

A-**B**. Comparison of transduction efficacy between AAV9 and LICA1 in all three muscles that were tested, in terms of VCN (**A**), and µDys RNA level (**B**). **C.** Comparison of percentage of successfully transduced

(dystrophin-positive) fibers in all three muscles that were tested. Note that TA, Qua, Dia muscles are presented in increasing order of severity. **D-E**. Comparison of restoration levels in dystrophic histological features between AAV9 and LICA1 in all three muscles that were tested, in terms of percentage of centro-nucleated fibers (**D**) and fibrosis level (**E**). Illustrated images in **C-E** are of quadriceps muscles (scale bar: 100µm). **F**. Serum MYOM3 level – indicator of muscle damage – 4 weeks post-injection (n=5, one-way ANOVA). **G-I**. Comparison of functional restoration between AAV9 and LICA1 by Escape test – global force measurement (**G**, n=6), tetanus force of TA muscle (**H**, n=10-12), and twitch force of TA muscle (**I**, n=9-12). **K-N**. Comparison of restoration in global transcriptomic changes in quadriceps muscle between AAV9 and LICA1 (n=4, adjusted p-values < 0.05). **K**. The heatmap presents the log2 fold change (log2FC) in comparison to WT muscle for all 8717 DEGs found in mdx muscle (compared to WT). The log2FC values are illustrated in row Z-scores, colored from blue to red, arranged from lowest to highest. **L-N**. Volcano plots of multiple comparisons illustrate transcriptomic changes before and after AAV treatment. As a reference, 4216 downregulated and 4501 upregulated DEGs found in mdx were colored blue and red, respectively, in all volcano plots. Among these DEGs, the number of genes found to be significantly different in each pair-wise comparison were labeled in the upper corners. **L**. Volcano plots comparing mdx/WT transcriptomes. **M**. Volcano plots comparing mdx to AAV-treated transcriptomes, in which significant DEGs are the genes correctly restored after AAV treatment. **N**. Volcano plots comparing AAV treatment to WT, in which significant DEGs are the genes that are not or incompletely restored after AAV treatment.

Fig. 5

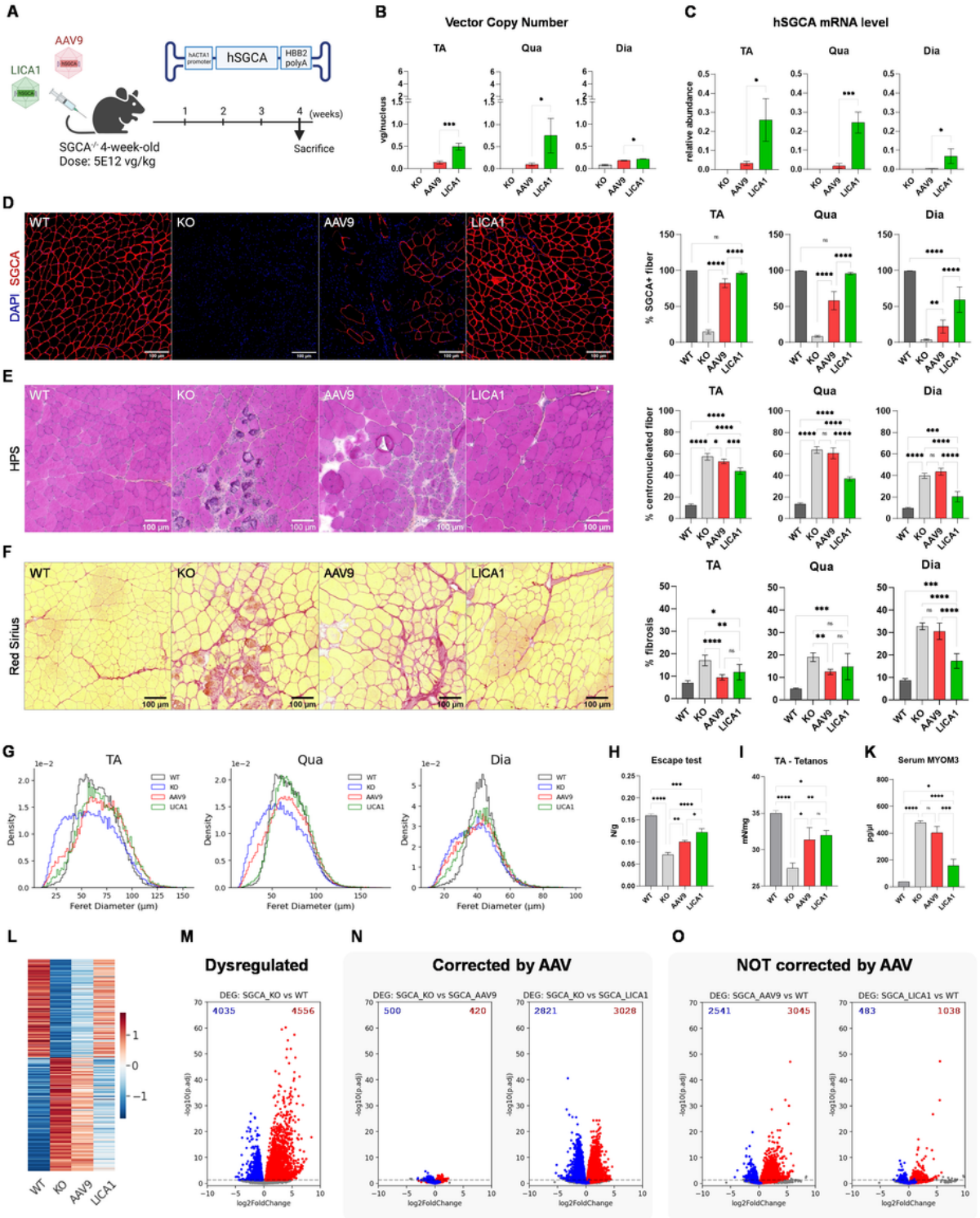

Figure 5

Low-dose gene transfer by LICA1 was better at restoring dystrophic phenotypes and functionality than AAV9 in the LGMDR3 mouse model.

A. Scheme of *in vivo* experiment: LICA1 (9rh74_4um9) or AAV9 were injected intravenously into a 4wo SGCA-KO mouse model at the dose of 5E12 vg/kg (expression cassette: hACTA1_hSGCA_HBB2-pA, n=3-

5). Three skeletal muscles in increasing order of severity, TA, Qua, and Dia, were analysed 4 weeks post-injection. **B-D**. Comparison of transduction efficacy between AAV9 and LICA1 in all three muscles that were tested in terms of VCN (**B**), hSGCA mRNA level (**C**), and percentage of succesfully transduced (SGCA-positive) fibers (**D**). **E-G**. Comparison of restoration levels in dystrophic histological features between AAV9 and LICA1 in all three muscles that were tested in terms of percentage of centro-nucleated fibers (**E**), fibrosis level (**F**), and fiber size distribution (**G**). Illustrated images in **D-F** are of quadriceps muscles (scale bar: 100 µm). **H-K**. Comparison of functional restoration between AAV9 and LICA1 using the escape test – global force measurement (**H**), tetanus force of TA muscle (**I**), and serum MYOM3 level – indicator of muscle damage (**K**). **L-O**. Comparison of restoration in global transcriptomic changes in quadriceps muscle between AAV9 and LICA1 (n=4, adjusted p values < 0.05). **L**. The heatmap presents the log2 fold change (log2FC) in comparison to WT muscle for all 8591 DEGs found in KO muscle (compared to WT). The log2FC values are illustrated by row Z-scores, colored from blue to red, arranged from lowest to highest. **M-O**. Volcano plots of multiple comparisons illustrate transcriptomic changes before and after AAV treatment. As a reference, 4035 downregulated and 4556 upregulated DEGs found in KO were colored blue and red, respectively, in all volcano plots. Among these DEGs, the number of genes found to be significantly different in each pair-wise comparison were labeled in the upper corners. **M**. Volcano plots comparing KO/WT transcriptomes. **N**. Volcano plots comparing KO to AAV-treated transcriptomes, in which significant DEGs are the genes correctly restored after AAV treatment. **O**. Volcano plots comparing AAV treatment to WT, in which significant DEGs are the genes that are not or incompletely restored after AAV treatment.

Supplementary Files

This is a list of supplementary files associated with this preprint. Click to download.

- ALICA1supp.pdf
- DatafileS2DEGSGCA.xlsx
- DatafileS1DEGDMD.xlsx